**_In-Vivo_ Confocal Evaluation of Corneal Nerves in Patients with Diabetic Neuropathy**


BY

Nilesh Raval


A thesis submitted in fulfillment of the Honors Biophysics Undergraduate Program in the
College of Literature, Science, and the Arts


at the


University of Michigan in Ann Arbor


December 20, 2013

**Table of Contents**

**Abstract**

*Purpose*: The objective of the first part of this study was to determine if the corneal nerve parameters of mean nerve count, total nerve length, percent primary nerve character, and tortuosity of nerves in the subbasal nerve plexus varied amongst three groups of patients: those with severe diabetic neuropathy, those with diabetes and mild to no clinical evidence of neuropathy, and a healthy control group.  The second part of this study focused on correlating nerve tortuosity values with mean nerve count, total nerve length, and primary nerve character.

*Methods*: Confocal data for patients with severe diabetic neuropathy (n = 7), diabetes and mild or no neuropathy (n = 15), and healthy controls (n = 9) were collected with the Heidelberg Retina Tomograph confocal microscope and analyzed using NeuronJ and CCMetric.  Image analysis included determining the mean nerve count, total nerve length, percentage of primary nerves, and tortuosity values for each scan.  Analysis of variance, Tukey's post-hoc test, and the Pearson Coefficient of Determination were used as tools for statistical analysis.

*Results*: There was a statistically significant difference ($p < 0.05$) in the mean nerve count between the healthy control group and the severe neuropathy group.  The healthy control group expressed a strong linear relationships when comparing tortuosity with mean nerve count ($R^2 = 0.77$) and mean nerve length ($R^2 = 0.64$), while the severe neuropathy group expressed its lowest values of mean nerve count and total nerve length at the highest and lowest tortuosity values.

*Conclusions*: The results support the hypothesis that corneal nerves, as imaged by confocal microscopy, correlate to, and can be used as diagnostic markers for, systemic diabetic neuropathy.  A larger patient sample size will increase confidence and reliability of the data, and an automated MATLAB script currently being developed will speed up the analysis process.

**Introduction**

Over 25 million people in the United States suffer from diabetes, and about 60-70% of diabetics express mild to severe forms of neuropathy [1]. In the past, the only method of directly examining the peripheral nerves was to conduct skin or nerve biopsies, which were uncomfortable and invasive. The benefit of using ophthalmic markers for early detection of diabetic peripheral neuropathy is that the procedure is non-invasive, cost-efficient, and clinically accessible. The first objective of this research is to compare the characteristics of corneal nerves – mean count, mean length, primary nerve character, and tortuosity – in patients with diabetes and severe neuropathy, diabetes and mild to no clinical evidence of neuropathy, and a healthy control group. The second objective is to determine how nerve tortuosity, a parameter that has not been studied extensively in the field, correlates with nerve count, length, and character. The ultimate goal of this study is to utilize the results as a quantitative diagnostic that can indicate the presence of diabetic neuropathy in patients before full expression of clinical symptoms of the disease arises.

The cornea can be easily examined in an outpatient setting using corneal confocal microscopy, an *in-vivo* procedure that involves shining a pinpoint laser into the patient's eye, progressively scanning through the layers of the cornea, and transmitting the scans to a digital imaging program to quantify the data. The presence of significant differences between groups of patients could hint at a pathophysiological mechanism relating the systemic condition of diabetes to the status of the corneal nerves. If significant correlations between diabetic neuropathy and corneal nerve parameters can be quantified, a model for the quantitative relationship between the severity of diabetic neuropathy and corneal nerve parameters can be established. This diagnostic model

could be utilized during routine doctor appointments or at regular eye exams to non-invasively test for early detection of diabetic neuropathy.

It is hypothesized that corneal nerves can be used as effective diagnostic markers for diabetic peripheral neuropathy, and that increased severity of neuropathy will correlate with lower nerve counts and lower total nerve lengths due to greater nerve damage in the cornea. It is also hypothesized that increased neuropathy will correlate with lower tortuosity values and a higher percentage of primary nerve character relative to secondary nerve character, due to the neuropathic destruction of the more tortuous secondary nerve branches that disrupts nerve-to-nerve communication. Finally, it is hypothesized that strong correlations will exist between tortuosity, nerve count, and nerve length in healthy patients but will not exist in neuropathy patients, as increased nerve damage may reduce the ability of the nerves to sense their surroundings and adapt to the presence of neighboring nerves by becoming more tortuous and compact.

**Background**

The cornea is the outermost layer of the front of the eye [2].  Completely transparent, its purpose is to refract light onto the retina in the posterior chamber of the eye.  The human cornea is comprised of five major layers: the epithelium, Bowman's layer, the stroma, Descemet's membrane, and the endothelium.  The epithelium is located on the outside of the cornea and makes up approximately 10% of the cornea's overall thickness [2].  The main functions of the epithelium are to protect the inner layers of the cornea from external debris such as dust particles and bacteria, and to provide a surface that is capable of absorbing the oxygen and cellular nutrients of tears and transmitting these nutrients to the inner layers.  The bottom layer of the epithelium, the basement membrane, serves as the anchor for epithelial cells.

Directly beneath the basement membrane lies Bowman's layer, an 8-14 μm thick, acellular layer composed of collagen [3].  The exact function of Bowman's layer has yet to be discovered, but it has been hypothesized that proper functioning of the human cornea is not dependent on this layer, as patients who have undergone excimer laser photorefractive keratectomy to remove Bowman's layer have not experienced any adverse effects [3,4].  The third layer, the stroma, accounts for 90% of the entire thickness of the cornea, and it is mainly comprised of water (~78%) and collagen (~16%) [2].  Stromal collagen is especially important for the maintenance of corneal structure, strength, and elasticity [2].  Descemet's membrane, a thin sheet of collagen fibers, lies directly behind the posterior stroma and serves as a protection against injury and infection.  The innermost layer of the cornea, the endothelium, is responsible for pumping out the excess fluid that leaks into the stroma from inside the eye, thereby safeguarding against edema and potential blindness [2].
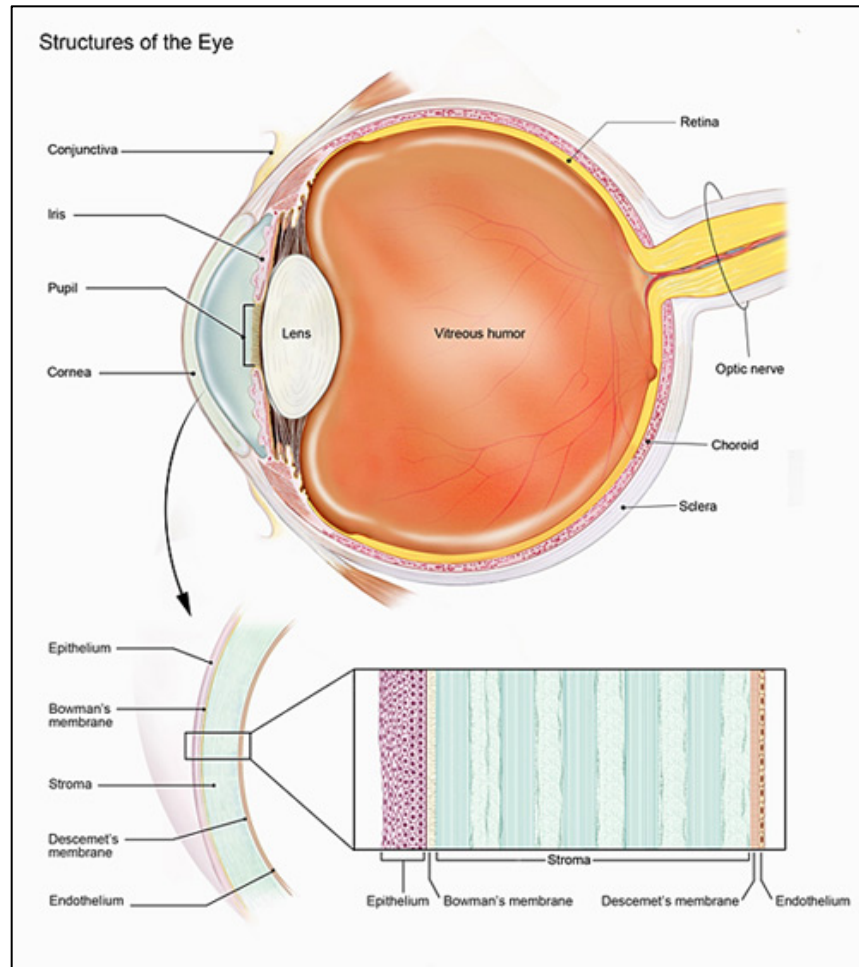
**Figure 1:** The five primary layers of the human cornea: epithelium, Bowman's membrane, stroma, Descemet's membrane, and endothelium [2].

Between the basal epithelium and Bowman's layer lies the subbasal, or subepithelial, nerve plexus, the corneal region responsible for epithelial innervation [5]. The subepithelial region of the human cornea contains a radiating pattern of bundles of nerve fibers that originate from stromal nerves and pass through small openings in Bowman's layer, converging in spiral-like patterns about 1-2 mm away from the corneal apex, the outermost point of the cornea [6]. The terminal endings of these nerve fibers reach the epithelial layer but are too small to be seen with contemporary confocal technology [6]. The nerve plexus consists of highly dense sensory and autonomic nerve networks, the former of which constitute the ophthalmic branch of the

trigeminal nerve [7]. Mechanical, thermal and chemical stimulation of these sensory nerves is the primary cause of pain in the human eye [7]. The autonomic network contains both sympathetic fibers, which are derived from the superior cervical ganglion, and parasympathetic fibers, which are derived from the ciliary ganglion [7]. The high density of nerve endings in the cornea is derived from the posterior ciliary nerves, and the cornea is approximately 100 times more sensitive than the neighboring conjunctiva [8]. If these nerve endings are destroyed, the cells of the epithelial layer will swell and produce basal lamina, which inhibits mitosis and directly causes apoptosis of epithelial cells [8].
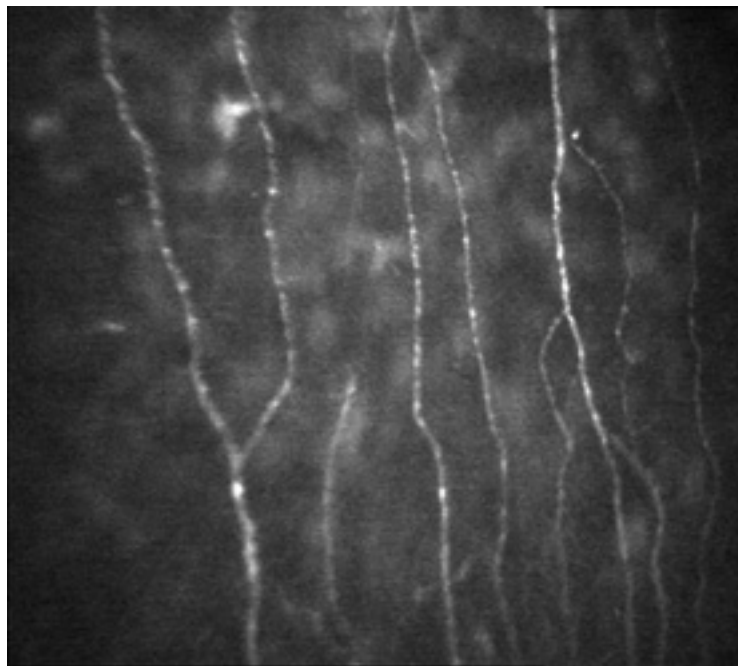


**Figure 2:** Subbasal nerve plexus, immediately anterior to Bowman's layer, as imaged by a confocal microscope [6]. The hyperreflectivity of Bowman's layer allows for easy characterization and visualization of the nerve plexus [9].

While nerves may also be found in the stromal layer, they are often much thicker than nerves in the subbasal nerve plexus, and can be differentiated from subbasal nerves as such [9]:
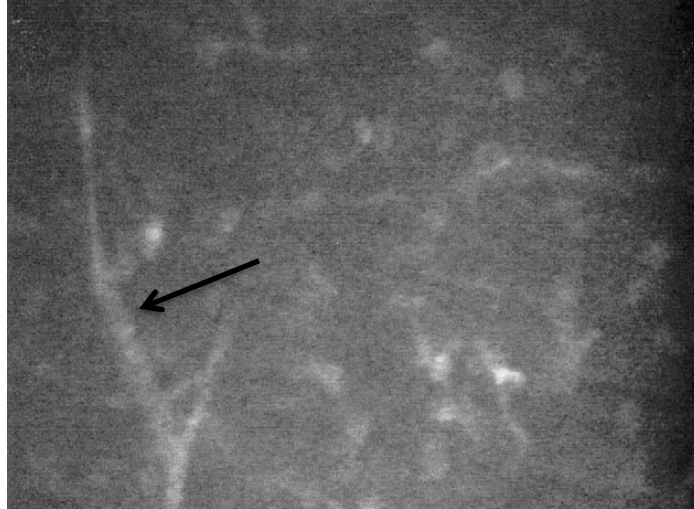
**Figure 3:** Stromal nerves are thicker than their subbasal counterparts [9]

An *in-vivo* study of corneal nerve morphology using a Confoscan slit-scanning confocal microscope showed that corneal nerves originate in the stroma with thick, linear trunks that extend both laterally throughout the stroma and towards the anterior part of the stroma [10]. Before these trunks reach the subbasal nerve plexus, they begin to thin out and form networks that extend towards, and penetrate through, Bowman's layer.

Diabetic neuropathy is nerve damage characteristic to patients with diabetes, as high blood sugar can damage nerves throughout the body [11]. This nerve damage is mainly the result of a combination of several systemic-based causes, including neurovascular, metabolic, and autoimmune factors. Prolonged exposure to high levels of blood glucose can damage the blood vessels that are responsible for carrying nutrients and oxygen throughout the body as well as cause inflammation in nerves [12]. The most common regions of nerve damage are in the nerves of the lower extremities, but studies have shown that this peripheral degeneration correlates with certain ophthalmic markers, such as the morphological degradation and reduced sensitivity of

corneal nerves, thinning of retinal nerve fibers, and peripheral field loss [13]. This project focuses on the first marker, corneal nerve degradation, and seeks to correlate key parameters of this effect, such as nerve count, nerve length, and tortuosity, with severity of diabetic neuropathy.

*In-vivo* corneal confocal microscopy is a technique that can be used to obtain a high-resolution scan of the human cornea. While the slit lamp biomicroscope and ophthalmoscope are also used by clinicians to observe the cornea, they are unable to do so with high clarity, detail, or magnification, and so physiological studies of the cornea at the microscopic level have been limited to *in-vitro* observations [14]. Light biomicroscopy of corneal layers results in poorly resolved images, because light is reflected from structures above and below the layer of interest [9]. For example, if a biomicroscope was used to examine a corneal lesion in the anterior stromal layer, light reflected from the surrounding layers – the epithelium, the tear film, and even the endothelium – would cause light contamination and defocus the target layer [9]. The corneal confocal microscope works on the principle of point illumination, whereby a light source and camera can be used simultaneously to illuminate and image a specific region of tissue in coplanar fashion [4]. The resolution of the image captured by a confocal microscope is therefore much higher than that of a traditional fluorescence microscope, which shines light evenly over an entire region rather than focusing it on a particular point. Since confocal microscopy only deals with one point of a sample at a time, the field of view from a single image will be negligibly small. To account for this potential problem, the confocal microscope "scans" over a small region of tissue by illuminating it with thousands of tiny points of light, so that a high-resolution, substantial field-of-view image of the region can be constructed via amalgamation of all of the

points in the plane. The confocal microscope can sequentially raster across each plane through

the z-axis, thus producing a series of cross-sectional images of the sample:
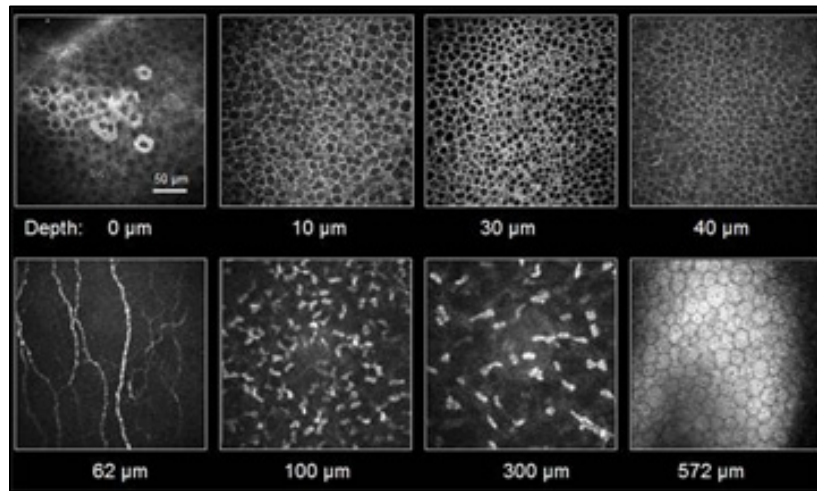


**Figure 4:** A cross-sectional view of the human cornea as viewed by a corneal confocal microscope. The epithelium (scans 1-4), nerve plexus (scan 5), anterior and posterior stroma (scans 6 and 7), and endothelium (scan 8) can be seen as the microscope scans through the cornea [15].

The United States Food and Drug Administration (FDA) has approved three types of confocal

microscopes for use in the clinical setting: the tandem scanning confocal microscope (TSCM),

the scanning-slit confocal microscope (SSCM), and the laser scanning confocal microscope

(LSCM) [16]. In the TSCM, the illumination and detection beams do not follow the same path;

rather, they travel tandem to one another through separate but identical apertures [17]. The main

advantages of the TSCM include its ability to image peripheral corneal lesions, capture real-time

images at up to 30 frames per second, and scan through the z-axis with high resolution [16, 18].

It does this via a Nipkow disc, which rotates at about 900 revolutions per minute and has 64,000

pinholes arranged in spiral fashion [18]. The SSCM, which works by eliminating out-of-focus

light from the scan via an array detector, is the most popular clinical confocal microscope due to

its user-friendly image analysis software [16]. Wide variations in subbasal nerve density have

been reported by several studies depending on the type of confocal microscope used.  The TSCM and the SSCM have measured nerve densities of healthy patients in the range from 5.5 $\mu$m/mm$^2$ to 11.1 $\mu$m/mm$^2$, while the LSCM has measured densities up to 21.7 $\mu$m/mm$^2$ [6].  The reason for these discrepancies lies in the differences in field brightness and image contrast amongst microscopes; the LSCM and SSCM tend to have greater brightness and contrast than the TSCM [6].  In addition, due to the high-resolution capabilities of the LSCM, it is able to detect smaller-caliber nerves, which is why its density estimates can be up to twice those of the SSCM [6].  Clear nerve detection is more difficult at the edges of images due to a decrease in field brightness [6], but error can be minimized if measurements are made in consistent fashion and the regions of interest for each image have the same areas.

The most recent confocal microscope and the one that has been used for this study is the LSCM (Heidelberg Retina Tomograph II Rostock Corneal Module, HRTII) [4].  The main advantage of using the HRTII over more traditional microscopes like the Confoscan series is that it is able to produce a series of extremely high-resolution, thin-layer images of the cornea.  HRTII generates high-contrast images at a wavelength of 670nm [6, 15]. Figure 5 below shows how a beam of laser light is directed through an initial aperture and a partial mirror, passes through a lens, and is directed through the focal plane of the lens onto a small section of the patient's cornea.  This light is then reflected off the cornea and travels back through the lens and through the partial mirror.  Another aperture with a small pinhole is placed adjacent to the mirror such that only the light that is coplanar with the focal plane of the lens is able to pass through to the detector.  This is specifically what makes confocal microscopy unique; the additional pinhole placed within the focal plane before the detector eliminates any out-of-plane light rays from flooding the detector.
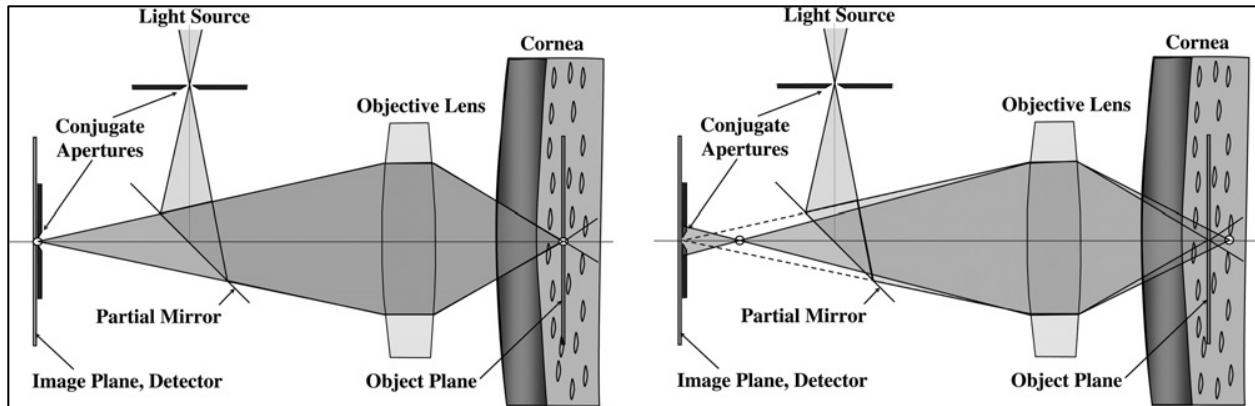
**Figure 5**: Basic layout of corneal confocal microscopy [6]. *Left*: the light rays at the focal point of the lens reflect off the cornea and are transmitted through the conjugate aperture to the detector. *Right*: the light rays that are not reflected off the object plane (dotted lines) are not transmitted through the conjugate aperture to the detector.

The left side of Figure 5 shows how light that is reflected at the focal point of the objective lens is "co-focused" and confocal to the detector. The right side of Figure 5 depicts the light rays that are out of the plane of the focal point of the objective lens (slightly anterior or posterior to the focal point) as solid lines that are defocused at the detector [6]. In other words, these rays are not coplanar to the lens and so the light rays reflected off this plane will not be transmitted through the pinhole to the detector. The lens can therefore be adjusted such that the cornea of the patient is located precisely at its focal point. The brightness of confocal images is dependent on several factors, such as the intensity of the laser, the radius of the confocal aperture, and the light scatter and specular reflectivity [6]. Small particles in the epithelial and stromal layers contribute to light scatter, while sudden changes in refractive index, which occur at the boundaries of the epithelial and endothelial layers, contribute to specular reflection [6].

Statistical analysis of the data obtained from NeuronJ and CCMetrics will consist of a One-Way Analysis of Variance (ANOVA), Tukey's post-hoc test, and the Pearson Coefficient of

Determination. The first two tools, ANOVA and Tukey's post-hoc test, will be used on the data

obtained from the first part of this study, where the corneal nerve parameters of mean nerve

count, total nerve length, tortuosity, and percentage of primary nerve character, are compared

across patient groups. The third tool, the Pearson Coefficient of Determination ($R^2$ value), will

be used during the multivariable portion of this study, where tortuosity is plotted against mean

nerve count, total nerve length, and percentage of primary nerve character for each patient group.

When comparing two samples, the t-test can be successfully utilized between the groups.

However, the problem with using the t-test when more than two groups are involved, as is the

case in this study, is that false positives tend to arise more often, and an error of $1 - (0.95)^n$

results, where n is the number of separate t-tests being conducted. One-way ANOVA corrects

this error by comparing all three means simultaneously instead of pair-wise, thereby eliminating

the added type I error probability that arises from performing multiple t-tests. ANOVA works by

generating an F statistic, or F value, which is defined as the variance between sample means

divided by the combined variance within each sample as shown in Equation 1 below [20]. The

p-value can be determined directly from the result of the F test via a correspondence table; the

program Windows OriginLab, automatically converts this F value to its corresponding p-value.

$$F = MS_{bg} / MS_{wg}$$

**Equation 1:** The F statistic as calculated by one-way ANOVA is defined as the ratio between the "mean square between groups" and the "mean square within groups." Mean square simply signifies the sum of the squares of the values between or within groups divided by the number of degrees of freedom between or within groups [20].

The null hypothesis of the F test is that the means of the samples are all equal. If the p-value that

results from the ANOVA test is greater than 0.05, this indicates that none of the mean values of

the groups are significantly different than the others.  However, if the p-value is less than 0.05,

this signifies that one or more of the groups has a significantly different mean value than the

others.  Since an ANOVA p-value less than 0.05 does not identify which specific groups are

significantly different from one another, Tukey's test, one of several post-hoc tests, can be used

to compare the groups pairwise (severe neuropathy and mild or no neuropathy groups, severe

neuropathy and healthy control groups, and mild or no neuropathy and healthy control groups)

without inducing any Type I error.  Tukey's test works based on a value called the Honest

Significant Difference, or HSD [20].  First the test calculates a studentized range statistic (Q),

which is defined as follows:

$$Q \ = \ \frac{M_L - M_S}{\mathrm{sqrt}\left[ MS_{wg} \Big/ N_{p/s} \right]}$$

**Equation 2:** Studentized range statistic as calculated by Tukey's post-hoc HSD test [20]. $M_L$ and $M_S$ are the larger and smaller means for each pairwise comparison, $MS_{wg}$ is the combined variance within each sample as calculated by ANOVA, and $N_{p/s}$ is the number of values per sample.  If these values are not all equal, the harmonic mean of the sample sizes can be determined instead [20].

For the 0.05 level of significance, which is used in this study, Windows OriginLab generates

critical values of Q, or values of the statistic that required for significance.  The HSD test in turn

uses these critical values to determine the magnitude of the difference between the means of the

two samples needed to be considered "significant" [20].  In other words, Equation 2 above is

rearranged to solve for the difference between $M_L$ and $M_S$ for the 0.05 level.

The last tool used in the statistical analysis portion of this study, the Pearson Coefficient of Determination, or $R^2$ value, gives a measure of the strength of the correlation between variables. In other words, the $R^2$ value is the percent of the variation in the y-value that can be explained by the variation in the x-value [21]. As a general method of determining the qualitative strength of the correlation from the coefficient value, the following protocol is used [21]:

| R value range | $R^2$ Value Range | Qualitative Strength of Correlation |
|---|---|---|
| > 0.90 | > 0.81 | Very Strong |
| 0.68 – 0.90 | 0.46 – 0.81 | Strong |
| 0.36 – 0.67 | 0.13 – 0.45 | Moderate |
| < 0.36 | < 0.13 | Weak |

**Table 1:** Qualitative strength of correlation as determined by the value of Pearson's Coefficient of Determination [21]. This system will be used to describe the correlations in this study.

**Materials/Methods**

The confocal data of 31 patients in a prospective clinical study at the Kellogg Eye Center in Ann

Arbor, MI were included in this analysis.  The patient sample consisted of three groups: those

with diabetes and proven severe neuropathy (n = 7), those with diabetes and mild or no clinical

evidence of neuropathy (n = 15), and an age-matched healthy control group (n = 9).  The

Heidelberg Retina Tomograph (HRT) was used to acquire confocal images of all the corneal

layers in each patient.  Five representative scans of the subbasal nerve plexus from the central

cornea were extracted for analysis for each patient.  These scans were analyzed using NeuronJ, a

nerve-tracing plugin of the image-processing program ImageJ, as depicted in Figure 6 on the

next page.  Image analysis included determining the mean number and length of nerves as well

as giving a breakdown of the type and percentage of nerves – primary, secondary, or tertiary

nerves – in the region analyzed for each patient.  A second image analysis program specific to

the assessment of corneal nerves of the subbasal nerve plexus, CCMetrics, was used to collect

the tortuosity data for each patient.  CCMetrics contains a built-in algorithm that accumulates the

nerve tortuosity values as each successive nerve is traced within a scan.  The greater this

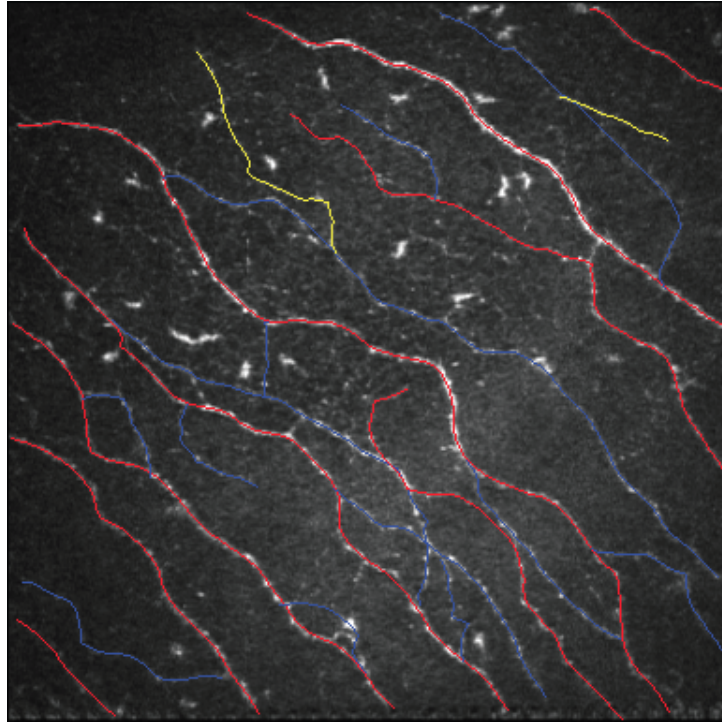tortuosity value, the greater mean nerve curvature exists in a given scan.

**Figure 6**: NeuronJ Tracing Software (ImageJ Plugin). The subbasal nerve plexus region shown above, captured by the HRT confocal microscope, has an area of $0.16mm^2$. The red lines signify primary nerves, the blue lines secondary nerves, and the yellow lines tertiary nerves. The white specks are corneal dendrites and were not assessed in this experiment.

The means and standard deviations of the nerve counts, nerve lengths, and tortuosity values across the three patient groups were collected and graphed. Statistical analysis was performed with Windows OriginLab and Microsoft Excel. ANOVA tests in Windows OriginLab were first used to compare the differences in mean nerve count, total nerve length, and nerve tortuosity among the three groups of patients. If the null hypothesis of the F test was rejected ($p < 0.05$), Tukey's post-hoc test was used to determine statistically significant differences between groups in pairwise fashion. The relationships between tortuosity and other parameters studied for these patients (mean nerve count, total nerve length, and percent primary nerve character) were plotted for the three groups to determine how these correlations varied based on severity of neuropathy.

To calculate the strength of each correlation, the Pearson Coefficient of Determination, or $R^2$ value, was determined for each regression plot, and the LINEST function in Microsoft Excel was used to give an estimate of the error in the slope and y-value.

**Results/Discussion**

The first objective of this study was to determine how the measured corneal nerve parameters of

mean nerve count, total nerve length, and nerve character varied by level of systemic neuropathy.

The one-way ANOVA test was conducted using the Windows Program Origin; if, and only if, a

p-value less than 0.05 was returned, the Tukey post-hoc test was used to determine the pairs of

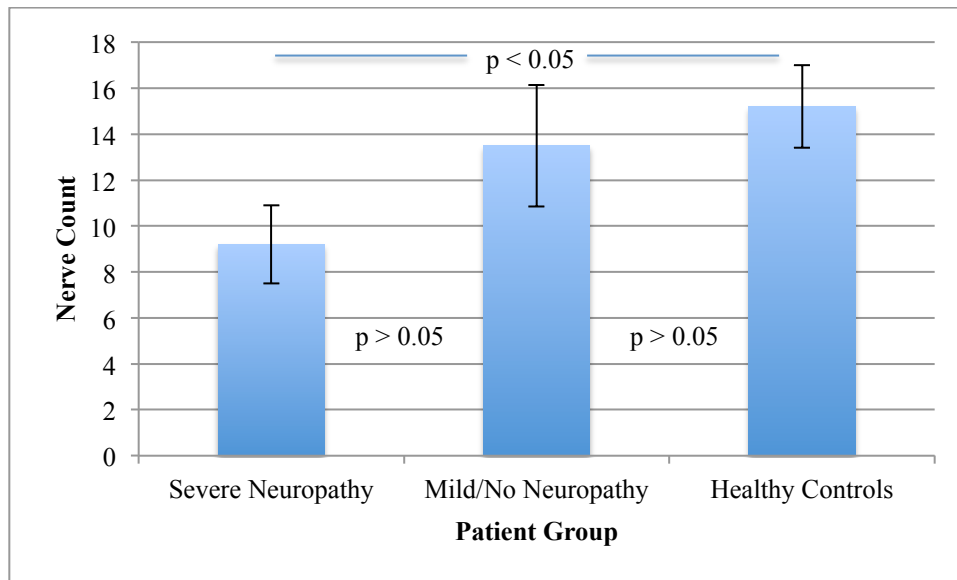groups that were significantly different from one another.  These results are shown below.



**Figure 7**: Mean nerve count amongst patient groups.  Tukey's post-hoc test shows
that there is a statistically significant difference between the mean nerve count of
the severe neuropathy patients (n=9.2) and that of the healthy control group
(n=15.2).  The error bars represent a single standard deviation.

|  | Degrees of Freedom | Sum of Squares | Mean Square | F value | P value |
|---|---|---|---|---|---|
| Model | 2 | 148.374 | 74.187 | 3.668 | **0.038** |
| Error | 28 | 566.300 | 20.225 | - | - |
| Total | 30 | 714.674 | - | - | - |

**Table 2**: ANOVA test for mean nerve counts amongst patient groups
shows that at least one of the groups has a significantly different
mean nerve count than the others (p < 0.05).

|  | Healthy Controls | Mild/No Neuropathy | Severe Neuropathy |
|---|---|---|---|
| Healthy Controls | - | $p > 0.05$ | **$p < 0.05$** |
| Mild/No Neuropathy | - | - | $p > 0.05$ |
| Severe Neuropathy | - | - | - |

**Table 3**: Tukey's post-hoc test for mean nerve counts amongst patient groups shows that the count for the healthy control group is significantly different than the count for the severe neuropathy group ($p < 0.05$). The other pairs of groups show no such difference ($p > 0.05$).

According to the one-way ANOVA test for mean nerve count amongst patient groups, the population means are significantly different ($F(2,28) = 3.668$, $p = 0.038 < 0.05$). This signifies that at least one of the groups has a significantly different mean nerve count than the others. To hash out these groups, the Tukey post-hoc test was used and, as depicted in Table 3 above, showed that the difference in mean nerve count between the severe neuropathy group and the healthy control group was statistically significant ($p < 0.05$). This result provides quantitative support to Figure 7 above, and it suggests that determination of the mean nerve count alone is indeed a parameter by which the presence of neuropathy can be measured in patients.
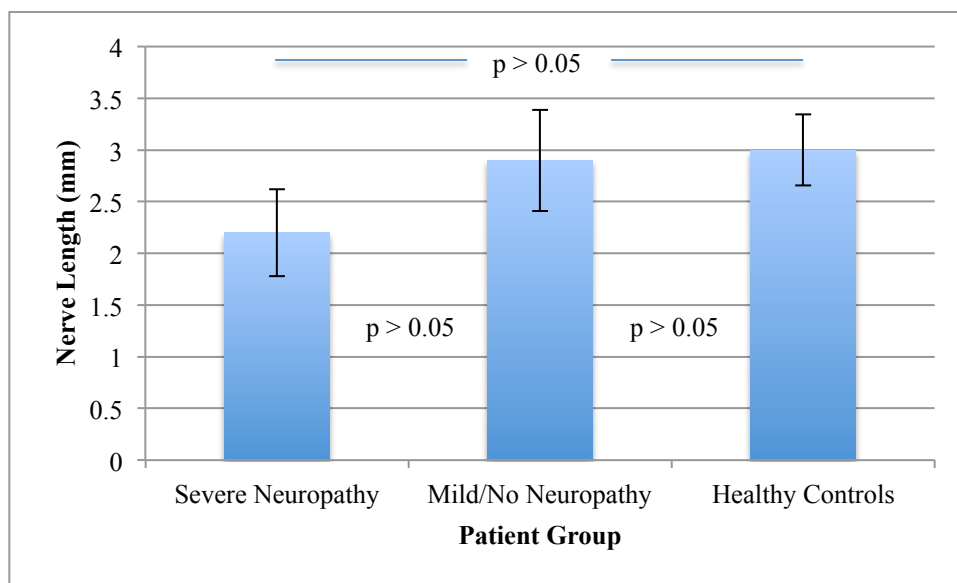


**Figure 8**: Total nerve length amongst patient groups. The ANOVA test shows that none of the groups have significantly different total nerve lengths than the other groups, which means that pairwise p values are all greater than 0.05. The error bars represent a single standard deviation.

|  | Degrees of Freedom | Sum of Squares | Mean Square | F value | P value |
|---|---|---|---|---|---|
| Model | 2 | 3.004 | 1.502 | 1.957 | **0.160** |
| Error | 28 | 21.488 | 0.767 | - | - |
| Total | 30 | 24.492 | - | - | - |

**Table 4**: ANOVA test for total nerve lengths amongst patient groups shows that p > 0.05, which means there is no statistically significant difference amongst the patient group.  Tukey's post-hoc test need not be carried out.

According to the one-way ANOVA test for total nerve lengths amongst patient groups, the population means are not significantly different (F(2,28) = 1.957, p = 0.160 > 0.05).  This provides quantitative support to Figure 8 above, and it suggests that determination of the total nerve length alone is not, in itself, a parameter by which the presence of neuropathy can be measured in patients.
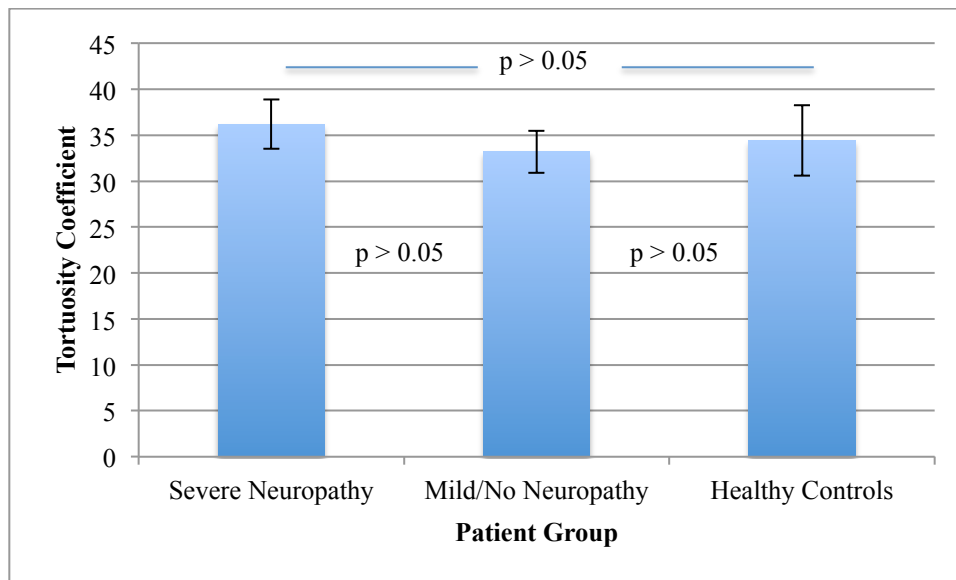


**Figure 9**: Tortuosity values amongst patient groups.  The ANOVA test shows that none of the groups have significantly different total nerve lengths than the other groups, which means that pairwise p values are all greater than 0.05.  The error bars represent a single standard deviation.

|  | Degrees of Freedom | Sum of Squares | Mean Square | F value | P value |
|---|---|---|---|---|---|
| Model | 2 | 43.339 | 21.670 | 0.650 | **0.530** |
| Error | 28 | 933.280 | 33.331 | - | - |
| Total | 30 | 976.619 | - | - | - |

**Table 5**: ANOVA test for tortuosity values amongst patient groups shows that p > 0.05, which means there is no statistically significant difference amongst the patient group. Tukey's post-hoc test need not be carried out.

According to the one-way ANOVA test for tortuosity values amongst patient groups, the population means are not significantly different ($F_{(2,28)} = 0.65$, $p = 0.53 > 0.05$). This provides quantitative support to Figure 9 above, and it suggests that determination of the tortuosity variable alone is not, in itself, a parameter by which the presence of neuropathy can be measured.

The following three figures are pie charts giving a breakdown of the nerve character (primary, secondary, or tertiary) within each patient group.
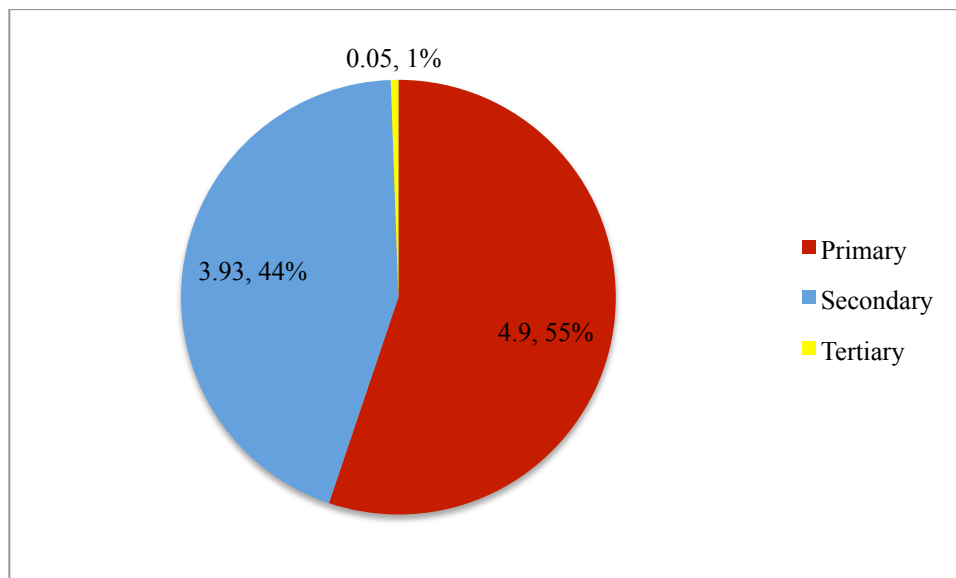


**Figure 10**: Prevalence of nerve character in severe neuropathy group. There was a greater number of primary nerves on average (count=4.90) than secondary nerves (count=3.93), with primary nerves constituting 55% and secondary nerves constituting 44% of the total nerve count.
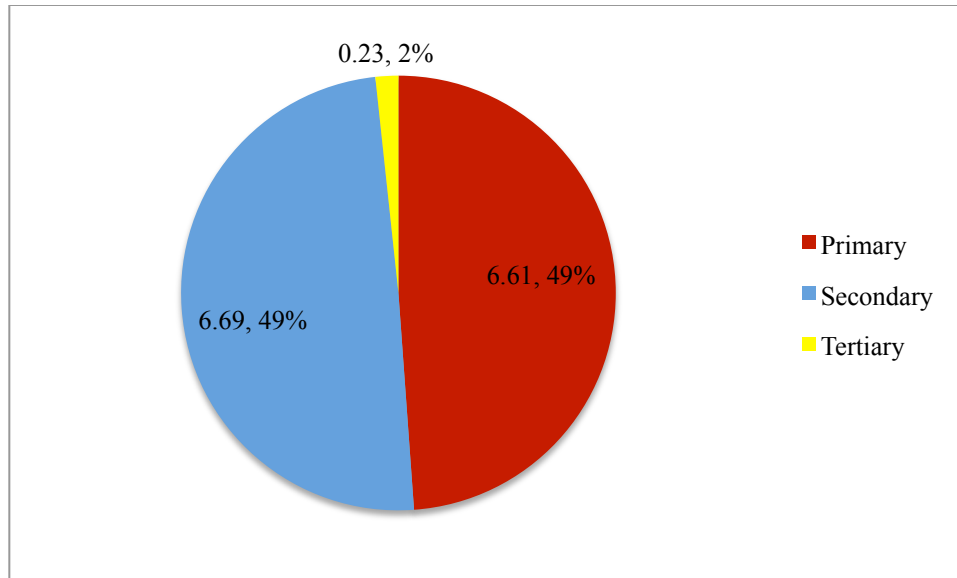
**Figure 11**: Prevalence of nerve character in mild/no neuropathy group. There was an approximately equal number of primary nerves (count=6.61) and secondary nerves (count=6.69), each sharing about 49% of the total nerves in this group of patients.
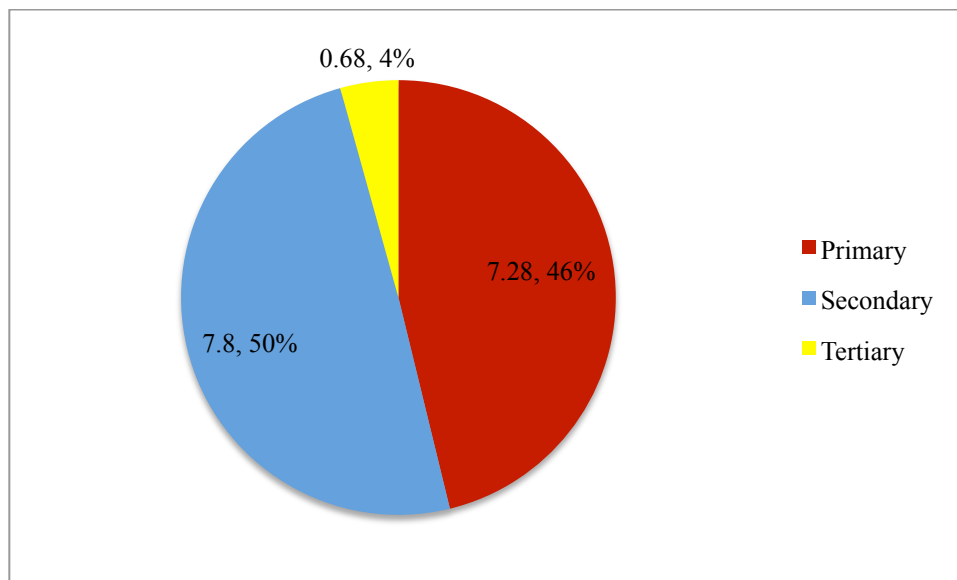


**Figure 12**: Prevalence of nerve character in the healthy control group. The mean number of primary nerves (count=7.28) was less than the number of secondary nerves (count=7.80), with the primary nerves comprising 46% of the total nerve count and the secondary nerves comprising 50% of the total count. The healthy patients exhibited more branched nerves on average than either of the diabetic groups.

Within the group of diabetes patients with proven, severe neuropathy, there were a greater number of primary nerves on average (count=4.90) than secondary nerves (count=3.93), with primary nerves constituting 55% and secondary nerves constituting 44% of the total nerve count. Tertiary nerves only contributed to approximately 1% of the total nerve count, with a mean number of 0.05 nerves. Within the group of diabetes patients with mild or no neuropathy, the number of primary nerves (count=6.61) and secondary nerves (count=6.69) were approximately equal, each sharing about 49% of the total nerves in this group of patients. Tertiary nerves only contributed 2% of the total nerve count, with a mean number of 0.23 nerves. Interestingly, within the healthy control group, the mean number of primary nerves (count=7.28) was actually less than the number of secondary nerves (count=7.80), with the primary nerves comprising 46% of the total nerve count and the secondary nerves comprising 50% of the total count. Tertiary nerves constituted 4% of the total nerve count, with a mean number of 0.68 nerves. Clearly, the healthy patients exhibited more branched nerves on average than either of the diabetic groups.

One possible explanation for the fact that there are a higher percentage of secondary nerves than primary nerves in the healthy control group and a lower percentage of secondary nerves than primary nerves in the severe neuropathy group is that the corneal nerves of healthy patients can cross-communicate more effectively. Secondary nerves, which branch directly off primary nerves and frequently bridge between pairs of nerves, are responsible for spreading action potentials that come from the trigeminal nerve across the entire subbasal nerve plexus. In patients with severe diabetic peripheral neuropathy, these secondary nerves are damaged via the pathophysiological mechanism of the disease, thereby disrupting this efficient communication method. This explanation is merely a hypothesis, however, and is by no means definitive.

The second objective of this study was to determine whether correlations exist between nerve tortuosity and other parameters, such as mean nerve count, total nerve length, and percent primary nerve character among the three different groups.  This part of the study has the potential to provide insight into the multivariable effects of diabetic neuropathy, namely, how the tortuosity value (deemed "tortuosity coefficient" by CCMetric) correlates with each of the nerve parameters.  As tortuosity is an aspect of nerve character that has been studied very little in the past, analyzing its relationship with nerve parameters can be used to explain nerve behavior in the subbasal nerve plexus. The following plots depict the relationships between tortuosity and these nerve parameters.  Vertical and horizontal error bars are given as the standard errors of the means of the nerve count and tortuosity values, respectively.
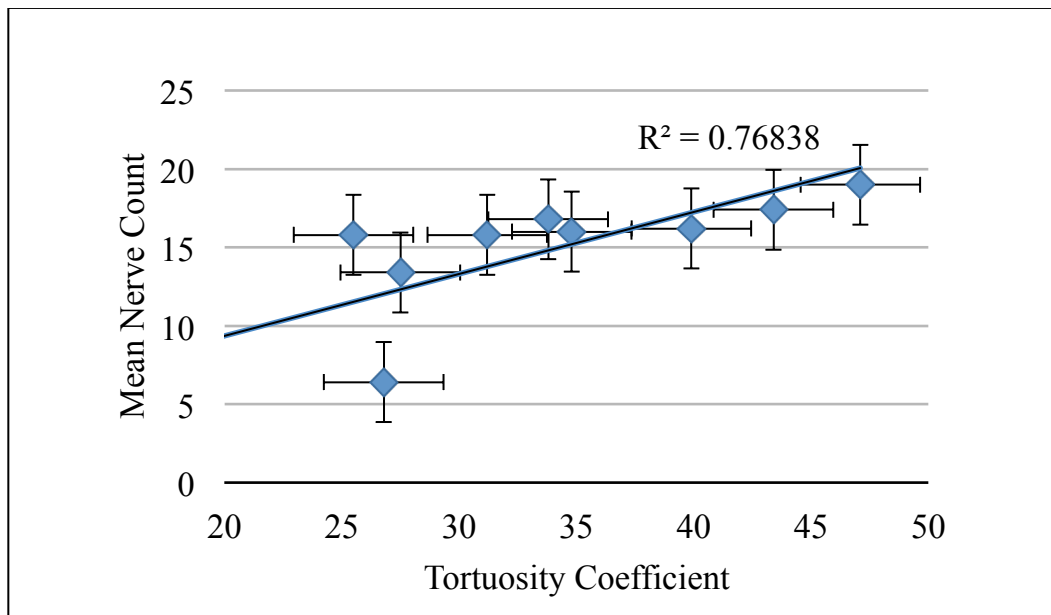


**Figure 13:** Mean nerve count vs. tortuosity in the healthy control group. The Pearson value shows that there is a very strong, positive correlation between these two variables. There is a slight positive correlation between tortuosity and nerve count, perhaps suggesting that greater nerve curvature allows for a more efficient packing of nerves within a given region of interest.  This relationship, however, is not necessarily causal.

| LINEST Information | Value |
|---|---|
| Slope | 0.309834804 |
| Standard Deviation of Slope | 0.135314952 |
| Standard Deviation of Y-Values | 2.926879049 |

**Table 6:** LINEST Function for Figure 13.  The standard deviations of the slope and Y-values are measurements of error within the regression plot.

Figure 13 shows that for the healthy patient group, tortuosity is directly proportional to mean nerve count.  There tends to be greater variability in the mean nerve count at lower tortuosity values than at higher tortuosity values as can be seen by the larger residuals for the first two points.  The $R^2$ correlation value of 0.768 signifies that there is a 76.8% chance that the data points are actual solutions to the line of the best fit.  The LINEST function in Microsoft Excel can be used to determine the numerical value of the standard deviation of the y-values.

The relationship between tortuosity and mean nerve count for the severe neuropathy group shows a much different correlation.  Worth noting is the unique, negative fourth-order polynomial shape of Figure 14 below.  Although it could be coincidence that this plot has this specific shape, especially given the small number of patients in the study group, it is important to note that the extreme values of tortuosity correlate with the lowest values of nerve count, with intermediate tortuosity values yielding greater nerve counts.   One must be careful not to draw a large number of conclusions from such a small sample of patients, and further studies should be carried out using a larger sample size to verify this finding.
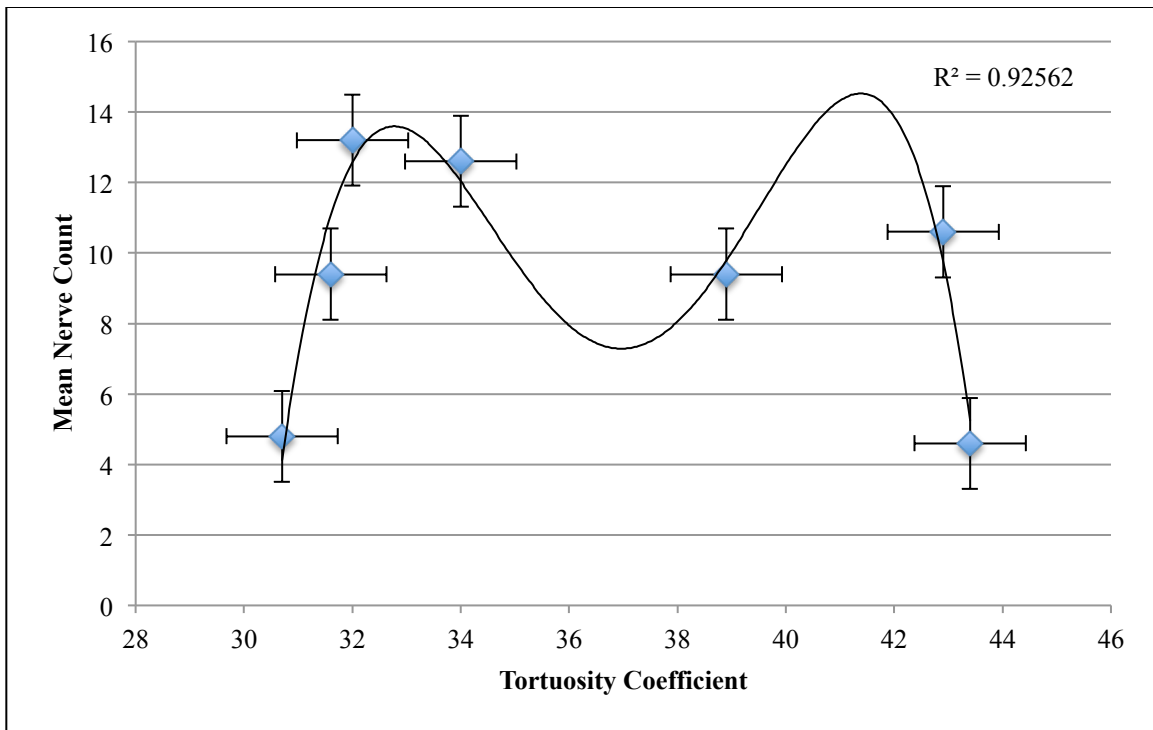
**Figure 14:** Tortuosity vs. mean nerve count in the severe neuropathy group. Although the negative, fourth-order polynomial shape of the best-fit curve may be coincidence, it is worth noting that the highest and lowest values of tortuosity correspond with the lowest mean nerve counts.

Although the correlations depicted above between mean nerve count and nerve tortuosity do not necessarily signify causation, there are still possible explanations that exist for why the relationship in the healthy group is positive and why the relationship in the severe neuropathy group is not. One possible line of reasoning for these correlations is that perhaps neuropathy causes a lack of communication or signaling between the nerves, so that even if there are a greater number of nerves within the subbasal nerve plexus of individuals with severe neuropathy, these nerves are not able to successfully communicate with one another and thus fail to accommodate for the increased nerve density by increasing their curvature, or tortuosity. Healthy individuals retain this ability for nerves to cross-communicate and therefore as mean nerve count increases, the tortuosity also increases, as nerves are able to effectively "sense" their

surroundings and accommodate by becoming more compact.  Again, this is by no means a

definitive account of what is actually happening; it is merely speculation by hypothesis and

reasoning.

For the healthy group, it was found that there is a direct correlation between tortuosity and total

nerve length, with greater nerve curvatures showing up in patient scans with greater total nerve

lengths.  This finding was similar to that made between tortuosity and mean nerve count.
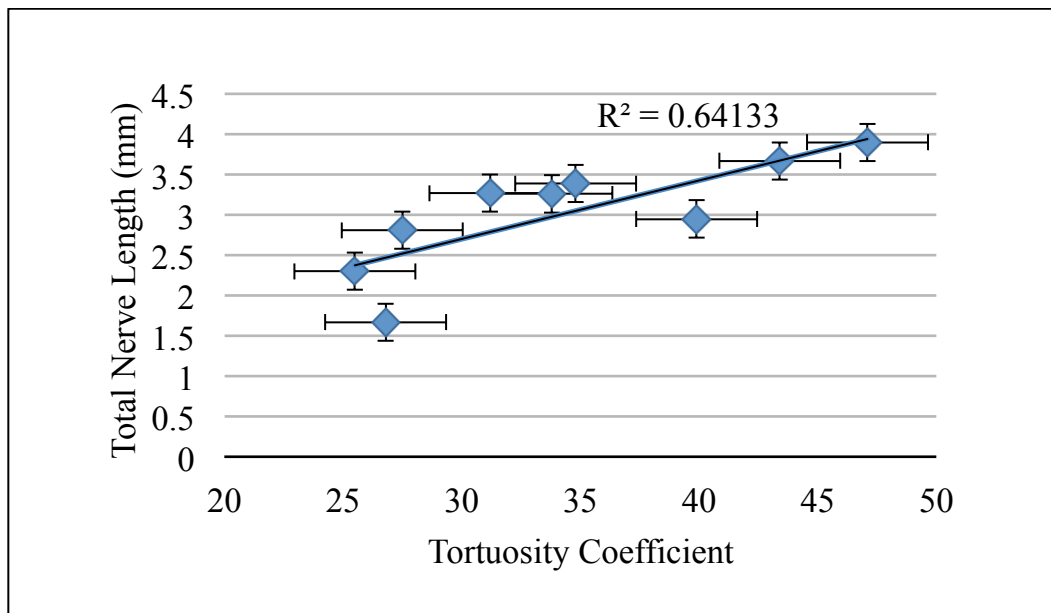


**Figure 15:** Tortuosity vs. total nerve length in the healthy group.  The Pearson value shows that there is a strong, positive correlation between these two variables, once again suggesting (but in no way proving) that greater nerve curvature could lead to a higher abundance of nerves within a region.

| LINEST Information | Value |
|---|---|
| Slope | 0.072585946 |
| Standard Deviation of Slope | 0.020516777 |
| Standard Deviation of Y-Values | 0.443780407 |

**Table 7:** LINEST Function for Figure 15.  The standard deviations of the slope and Y-values are measurements of error within the regression plot.

Severe neuropathy patients with greater tortuosity values also showed a negative, fourth-order polynomial correlation with total nerve length, similar to the relationship displayed in Figure 14.
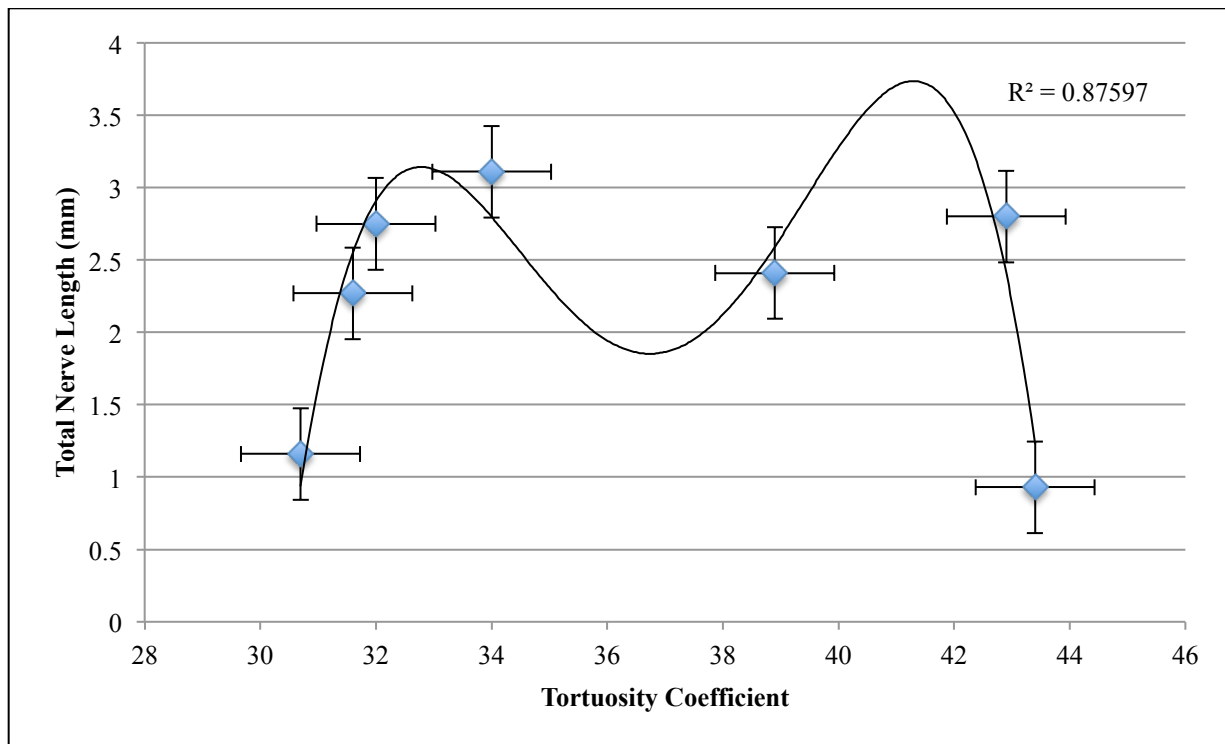


**Figure 16:** Tortuosity vs. total nerve length in the severe neuropathy group. Although the negative, fourth-order polynomial shape of the best-fit curve may be coincidence, it is worth noting that the highest and lowest values of tortuosity correspond with the lowest total nerve length.

Since total nerve length and mean nerve count within a scan are related to nerve density, the reasoning that the nerves of patients with severe peripheral neuropathy are not able to communicate as effectively as those of healthy patients and curve more in regions of higher nerve densities makes intuitive sense.

There is another unique characteristic about the healthy control group that fails to show in either of the other two groups. With respect to tortuosity coefficient versus percentage of primary nerves (out of total number of primary, secondary, and tertiary nerves), the healthy control group shows a moderately-strong negative correlation as depicted in Figure 17, while there is no correlation present in the other two groups.
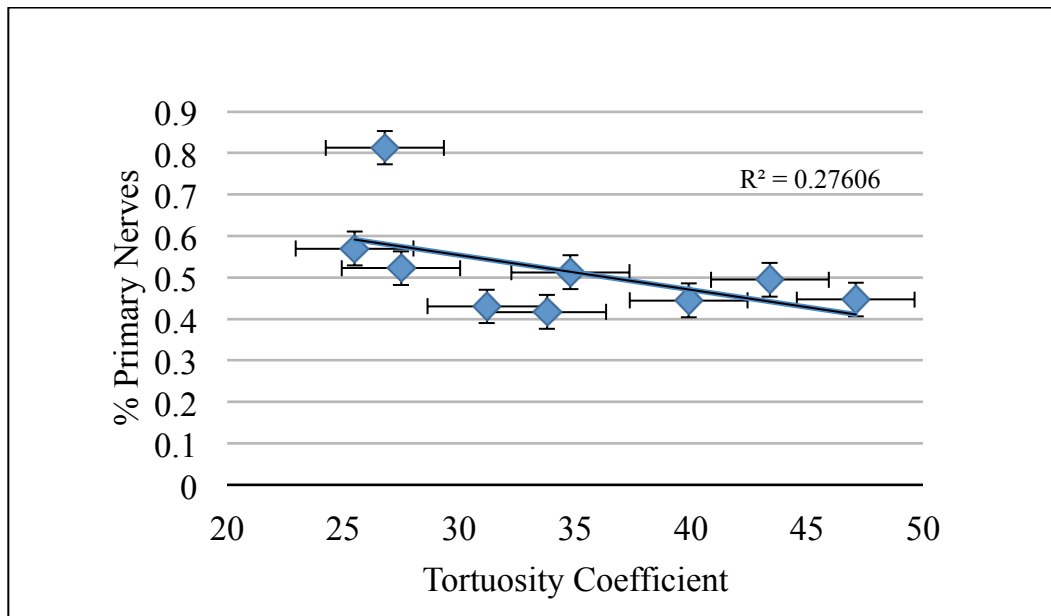


**Figure 17:** Tortuosity vs. percentage of primary nerves in the healthy group. The Pearson value shows that there is a moderate, negative correlation between these two variables.

| LINEST Information | Value |
|---|---|
| Slope | -0.008358811 |
| Standard Deviation of Slope | 0.005116213 |
| Standard Deviation of Y-Values | 0.110664317 |

**Table 8:** LINEST Function for Figure 17. The standard deviations of the slope and Y-values are measurements of error within the regression plot.

The moderately-strong, negative correlation between tortuosity and percentage of primary nerves within a given scan in the healthy group could be explained by the observation that primary nerves are generally less tortuous than secondary and tertiary nerves. This cannot, however, explain the lack of such a correlation within the groups with neuropathy. Looking at Figures 13-17 altogether, it seems that lack of any positive or negative linear correlation between tortuosity coefficient and other variables measured points toward a case of diabetic peripheral neuropathy.

Table 9 below outlines the correlations that were found when the tortuosity coefficient of the patients in each of the three groups of patients was plotted against corneal nerve and cell data that were collected for these same patients. The strongest correlations among the three groups appear to be the positive linear correlation in the tortuosity versus both mean nerve count and total nerve length in the healthy control group (as per Figures 13 and 15 above) and a lack of such a relationship in the other two groups. However, within the severe neuropathy group, there is a unique correlation that exists between the tortuosity coefficient and both mean nerve count and total nerve length. For this group, both the highest and lowest tortuosity values – the extremes – correlate with the lowest mean nerve count and shortest total nerve lengths.

Although it is not clear whether the values between these extremes approximate a negative parabola or negative fourth-order polynomial curve, it is evident in Figures 14 and 16 below that patients with severe diabetic neuropathy show the lowest values of nerve counts and nerve lengths at extreme tortuosity values.

| | **Severe Neuropathy** | | **Mild/No Neuropathy** | | **Healthy Controls** | |
|---|---|---|---|---|---|---|
| | Correlation | Strength | Correlation | Strength | Correlation | Strength |
| Tortuosity vs. Mean Nerve Count | Lowest mean nerve counts at extreme tortuosity values | $R^2 = 0.93$ (Very strong) | none | N/A | (+) linear | $R^2 = 0.77$ (Very strong) |
| Tortuosity vs. Total Nerve Length | Lowest total nerve lengths at extreme tortuosity values | $R^2 = 0.88$ (Very strong) | none | N/A | (+) linear | $R^2 = 0.64$ (Strong) |
| Tortuosity vs. % Primary Nerve Character | none | N/A | none | N/A | (–) linear | $R^2 = 0.28$ (Moderate) |

**Table 9**: Multivariable Corneal Correlations

**Conclusions**

*In-vivo* confocal corneal microscopy has proven to be an effective clinical method to assess the nerves in the subbasal nerve plexus of the cornea. The relationships between tortuosity and nerve count, nerve length, basal cell density, and percent primary nerve character have shown that there are correlative differences amongst healthy patients and those expressing forms of diabetic neuropathy. This study has shown that there is a statistically significant difference ($p < 0.05$) in the mean nerve count of corneal nerves between healthy patients and severe neuropathy patients, proving correct the hypothesis that patients with neuropathy express a lower mean nerve count. It has also shown that patients who express high tortuosity values along with high nerve counts and lengths, as depicted by the strong correlations in the multivariable study, are more likely to be healthy than those who express high tortuosity values with low nerve counts and lengths. A strong positive, linear correlation between tortuosity versus both mean nerve count and total nerve length, and a negative linear correlation between tortuosity versus primary nerve percentage, are not characteristic of patient groups that express some form of diabetic neuropathy.

This study can be improved in several ways. First, the patient sample size used was not large enough to elicit trends with great confidence. In future studies, each of the three groups should have the same number of patients, with at least 20 patients per group. In the current study, the severe neuropathy group only contained seven subjects, which makes it difficult to claim that the relationships between tortuosity and other nerve parameters are reliable. Once a large number of patients are sampled for this study, multivariable regression equations can be developed and used to determine a patient's level of neuropathy with a much higher confidence. This project can

also be improved by using an automated MATLAB script to perform rapid, reliable image analysis of patient scans rather than having to manually trace the nerves of each patient using NeuronJ and CCMetric. A MATLAB algorithm is currently being developed by a group of engineering students at the University of Michigan that sequentially runs through the confocal scans, defines a threshold value for each image, eliminates background noise (dendrites and microdots that are not needed for nerve analysis), and provides information on nerve parameters, such as nerve count and length, for each scan. Automating this process will speed up data analysis tremendously and allow for the confocal scans of large numbers of patients to be analyzed with greater precision. In future projects, the specificity and sensitivity of this updated model will be tested so that it can be used in the clinical setting as a valid diagnostic for diabetic neuropathy.

**Acknowledgments**

**References**

[1] "Diabetes Statistics." *Diabetes.org*. American Diabetes Association, 2012. Web. 3 Oct. 2013.

[2] "Facts About The Cornea and Corneal Disease." *National Institutes of Health*. National Eye Institute, May 2013. Web. 3 Oct. 2013.

[3] Lagali, Neil, Johan Germundsson, and Per Fagerholm. "The Role of Bowman's Layer in Corneal Regeneration after Phototherapeutic Keratectomy: A Prospective Study Using In Vivo Confocal Microscopy." *Investigative Ophthalmology & Visual Science* 50.9 (2009): 4192-198. 5 Oct. 2013.

[4] Tavakoli, Mitra, Parwez Hossain, and Rayaz A. Malik. "Clinical Applications of Corneal Confocal Microscopy." *Journal of Clinical Ophthalmology* 2.2 (2008): 435-45. Print.

[5] Masters, Barry R., and Andreas A. Thaer. "In Vivo Human Corneal Confocal Microscopy of Identical Fields of Subepithelial Nerve Plexus, Basal Epithelial, and Wing Cells at Different times." *Microscopy Research and Technique* 29.5 (2005): 350-56. *Wiley Online Library*. Web. 2 Oct. 2013.

[6] Erie, Jay C., Jay W. McLaren, and Sanjay V. Patel. "Confocal Microscopy in Ophthalmology." *American Journal of Ophthalmology* 148.5 (2009): 639-46. Web. 2 Oct. 2013.

[7] Al-Aqaba, Mouhamed A., Usama Fares, Hanif Suleman, James Lowe, and Harminder S. Dua. "Architecture and Distribution of Human Corneal Nerves." *British Journal of Ophthalmology* 94.6 (2010): 784-89. Web.

[8] Wells, Jill R., MD, and Marc A. Michelson, MD. "Diagnosing and Treating Neurotrophic Keratopathy." *EyeNet Magazine* 2013. Web. 2 Oct. 2013.

[9] Chiou, Auguste G.Y., MD, Stephen C. Kaufman, MD, PhD, Herbert E. Kaufman, MD, and Roger W. Beuerman, PhD. "Clinical Corneal Confocal Microscopy." *Survey of Ophthalmology* 51.5 (2006): 482-500. Print.

[10] Oliveira-Soto, L., and N. Efron. "Morphology of Corneal Nerves Using Confocal Microscopy." *Cornea* 20.4 (2001): 374-84. *PubMed*. US National Library of Medicine. Web. 2 Oct. 2013.

[11] "Diabetic Neuropathy." *Mayo Clinic*. Mayo Foundation for Medical Education and Research, 06 Mar. 2012. Web. 4 Oct. 2013.

[12] "Diabetic Neuropathies: The Nerve Damage of Diabetes." *National Diabetes Information Clearinghouse (NDIC)*. National Institutes of Health, 25 June 2012. Web. 16 Dec. 2013.

[13] Efron, N. "Ophthalmic Markers of Diabetic Neuropathy." *Optometry & Visual Science* 88.6 (2011): 661-83. *PubMed*. National Institutes of Health. Web. 4 Oct. 2013.

[14] Jalbert, I., F. Stapleton, and M. Coroneo. "In Vivo Confocal Microscopy of the Human Cornea." *British Journal of Ophthalmology* 87.2 (2003): 225-36. National Institutes of Health. Web. 7 Oct. 2013.

[15] "HRT Rostock Cornea Module." *Heidelberg Engineering*. Heidelberg Engineering GmbH, 2013. Web. 7 Oct. 2013.

[16] "Confocal Microscopy." *The Ophthalmic News & Education Network*. American Academy of Ophthalmology, 2013. Web. 7 Oct. 2013.

[17] Spring, Kenneth R., Thomas J. Fellers, and Michael W. Davidson. "Confocal Microscope Scanning Systems." *FluoView Resource Center*. Olympus Corporation, 2009. Web. 7 Oct. 2013.

[18] Dhaliwal, Jasmeet S., Stephen C. Kaufman, and Auguste GY Chiou. "Current Applications of Clinical Confocal Microscopy." *Current Opinion in Ophthalmology* 18.4 (2007): 300-07. Print.

[19] Patel, Dipika V., and Charles N.J. McGhee. "Contemporary in Vivo Confocal Microscopy of the Living Human Cornea Using White Light and Laser Scanning Techniques: A Major Review." *Clinical & Experimental Ophthalmology* 35.1 (2007): 71-88. Print.

[20] Lowry, Richard. *Concepts and Applications of Inferential Statistics*. Vassar Stats, 2013. Web. 9 Oct. 2013.

[21] Taylor, Richard, EDD, RDCS. "Interpretation of the Correlation Coefficient." *Journal of Diagnostic Medical Sonography* 6.1 (1990): 35-39. Web. 13 Oct. 2013.